MEASUREMENT OF THE ODIN TELESCOPE AT 119 GHz WITH A HOLOGRAM TYPE CATR

J. Ala-Laurinaho[1], T. Hirvonen[1], P. Piironen[1], A. Lehto[1], J. Tuovinen[1], A. V. Räisänen[1], U. Frisk[2]

[1]Radio Laboratory, Helsinki University of Technology,
P.O. Box 3000, FIN-02015 HUT, Espoo, Finland
[2]Swedish Space Corporation,
P.O. Box 4207, S-17104 Solna, Sweden

Abstract − Development work of a 119 GHz CATR, based on a 2.4 m × 2.0 m hologram, and its application on the Odin telescope tests are described. The hologram element comprises seven parts, which are fabricated using silk-screen printing techniques. Comparison between the theoretical and the measured quiet-zone fields of the hologram CATR is made, which demonstrates the correctness of the analysis method and also the importance of high-quality physical joints between the hologram parts. The CATR has been successfully used in the measurement of a 1.1 m offset reflector antenna onboard the Odin spacecraft. The measured and calculated antenna radiation patterns are in good agreement in the main beam region. The effects of the imperfections in the quiet-zone field and in the aperture field of the antenna on the measurement results are simulated.

1. Introduction

In a hologram type of compact antenna test range (CATR), the plane wave, necessary for antenna testing, is produced using a planar, computer-generated, binary-amplitude hologram as the collimating element [1,2]. The feed horn transmits a spherical wave illuminating one side of the hologram, which modulates the field such that a planar wave is emanated on the other side of the structure. Figure 1 illustrates the layout of the hologram CATR and shows an example of the binary-amplitude hologram used in CATRs.

The extent of the volume enclosing the plane wave is called the quiet-zone, which is where the antenna under test (AUT) is situated. The required field-quality of the quiet-zone is driven by the required measurement accuracy of the AUT, typical requirements being a peak-to-peak amplitude ripple of less than 1 dB and a peak-to-peak phase ripple of less than 10°. The advantage of the hologram CATR over its reflector-based counterpart is its less stringent surface accuracy requirement [1−3]. This is due to the fact that, in this application, the hologram is a transmission type of collimating element.

Helsinki University of Technology (HUT) participates in the Odin satellite project, which is a collaboration project between Sweden, Finland, Canada, and France led by the Swedish Space Corporation. The Odin satellite is being developed for measuring aeronomical and

astronomical molecular spectral lines [4]. The Odin satellite will be launched in February 2001. The satellite has a heterodyne receiver at 119 GHz and four heterodyne receivers at submillimeter wave frequencies between 486 and 580 GHz. The receivers are fed by an offset reflector antenna with a main reflector aperture diameter of 1.1 m (Figure 2). The telescope was tested at 119 GHz with the hologram type of compact antenna test range in Linköping, Sweden, during August 1998. This was the first demanding antenna measurement task utilizing the hologram CATR. The main goal of these measurements was to ensure that the beamwidth and symmetry of the main beam of the Odin telescope are as designed.

In this paper, the development work of the large 2.4 m × 2.0 m millimeter wave hologram for the Odin telescope tests is described. The quality of the CATR is assessed comparing the measured and the simulated quiet-zone fields. The applicability of the CATR in testing large millimeter wave antennas is demonstrated by the measurement results of the Odin satellite antenna. Finally, the effects of the imperfections in the quiet-zone field and in the aperture field of the antenna on the measurement results have been simulated and these results are presented.

2. Hologram for Odin Tests

2.1. Hologram Design

The binary structure of the amplitude hologram can be computed, when the input and the desired output fields are known [2,5]. The input field is the radiation pattern of the feed on the hologram plane. The output field has a flat phase distribution but the amplitude is tapered to avoid edge diffraction. In practice, even for binarized hologram, the transmission of the electromagnetic wave through a hologram is not binarized but depends on the polarization and the widths of the slots. Therefore, the hologram pattern optimization for the desired quiet-zone field is an iterative procedure, which is based on an appropriate simulation method for the transmitted field [2,6].

The simulation method is based on two-dimensional finite difference time domain (FDTD) and physical optics (PO) methods [2,6]. The transmission of the field through the hologram is simulated with FDTD and the aperture field of the hologram is determined. Then, the field in the quiet-zone extent is calculated from aperture field by means of PO. Because the geometry of the hologram varies slowly in the vertical direction, only one horizontal cut of the hologram is simulated at a time with FDTD, and the quiet-zone field at the same horizontal plane is calculated. To optimize the whole quiet-zone cross-section, the simulation has to be carried out for different horizontal planes. The optimization of the hologram for Odin tests was performed for four different planes, at the centerline and 250 mm, 500 mm, and 750 mm from the centerline.

The size of the hologram depends mainly on the required size of the quiet-zone and how the hologram is illuminated. In this case, a 2.4 m × 2.0 m elliptic hologram with 557 curved 0.1−1.3 mm wide slots was designed. The hologram is illuminated by a corrugated horn placed in the focus, 6.0 m away from the hologram. The quiet-zone field at vertical polarization is optimized for a distance of 6.0 m at the opposite side of the hologram. The plane wave leaves the

hologram at an angle of 33.0°. The design of the hologram for Odin telescope tests is described more thoroughly in [7].

2.2. Hologram Manufacturing

The optimized pattern of the hologram is printed on film with a high-precision plotter having a resolution of 760 dots per inch (pixel size 33 μm). The printed film is then used as a mask in the silk-screen printing process when the pattern is transferred to a copper plated Mylar sheet. The thickness of the Mylar sheet is 75 μm, and the copper layer is 35 μm. The relative permittivity of Mylar is 3.3. Lithographic processes (other than the silk screen printing), which are used for fabricating printed circuits, would be more accurate than the silk-screen printing but they are not capable of producing structures of the required size [7]. The RMS error in the slot widths due to the silk-screen printing process is estimated to be about 30 μm, which is seen adequate for this specific hologram.

Due to the limitations in the maximum size of the mask, silk screen printing, and the Mylar film, the hologram has to be composed of seven pieces as shown in Figure 3. The maximum size of one piece is 1.2 m × 1.0 m. Because it is highly desirable to avoid any kind of joints in the center of the structure, a maximum-size piece is set in the center area. The pieces are spliced together by using 50 mm wide and 30 μm thick polyester tape on both sides of the film [7].

2.3 Quiet-zone Field Measurements

The hologram CATR is tested at 119 GHz by moving a probe antenna across the quiet-zone with a linear scanner. The transmitter is a phase-locked Gunn oscillator and the receiver is a spectrum analyzer with an external harmonic mixer. With this measurement set-up only the amplitude can be measured.

Figure 4 a shows the theoretical and experimental quiet-zone amplitudes in the horizontal direction at the center of the quiet-zone. The curves have been vertically shifted in order to separate them from each other. The solid line is the optimized theoretical amplitude distribution. The line with the bullets is the theoretical amplitude distribution when the two vertical joints have been included in the analysis. The line with the stars is the measured amplitude distribution. Figure 4 b shows the theoretical phase distributions in the quiet-zone in the horizontal direction. Figure 4 c shows the measured quiet-zone amplitude in the vertical direction.

The theoretical, peak-to-peak amplitude and phase ripples are less than 1 dB and 10° at each of the four optimized horizontal cuts (the centerline-cut is shown in Figures 4 a and b). The measured peak-to-peak amplitude ripple is about 3 dB in the worst part of the quiet-zone and less than 1.5 dB in most parts of the quiet-zone. The extra amplitude ripple between the optimized and realized quiet-zone fields is caused by the joints of the hologram [7].

The theoretical analysis of the joints is done in such a way that the leftmost piece and the center piece are assumed to be too close to each other by 0.4 mm ('negative' gap), and a 0.4 mm 'positive' gap is introduced between the center part and the rightmost part. The tape is also included in the analysis model, and dielectric constant of 3.3 is used for the polyester tape. The effect is an increased amplitude ripple, especially in the portion of the quiet-zone where the joints radiate most, but also elsewhere in the quiet-zone. The flat phase area is reduced substantially. The exact amount of the displacement is not measured. However, the agreement between the theoretical and measured amplitudes is good. The effects of the joints are discussed more in [7].

The field quality in the quiet-zone is considered to be appropriate for measuring the Odin telescope at the main beam radiation pattern where, according to simulations, the amplitude ripple has a small effect. The effects of the unsatisfactory phase distribution in the quiet-zone are expected to be a reduction in the measured gain of the AUT, filling of the nulls, and increased sidelobe levels.

3. Measurements of the Odin Telescope

The purpose of the Odin telescope tests is to verify the radiation pattern of the antenna in the main beam region. Figure 5 shows the arrangement of the hologram CATR during the tests. The best place for the measurement set-up would be an anechoic chamber, but the space needed for the facility is so large that the CATR has to be placed in a large laboratory room. The surroundings of the hologram are covered with absorbers to block the direct radiation from the feed to the quiet-zone area. Also, a wall of absorbers is built to absorb the diffraction wave modes, which are radiated by the hologram and propagate mainly in the direction of the hologram normal.

The telescope is measured as a complete unit using its own 119 GHz receiver for detection. The direction of the plane wave in a CATR is steered by moving the feed antenna in the transverse plane (Figure 5). With this feed scanning, the main beam can be measured without need to rotate the AUT. The required feed scanning is ± 26 mm in the horizontal direction and ± 30 mm in the vertical direction corresponding to the plane wave rotation of ± 0.30° and ± 0.29°, respectively [7].

Figure 6 shows the radiation pattern of the Odin telescope as a contour plot. The separation of the contour lines is 3 dB. The measured radiation pattern is symmetric in the main beam region.

Figures 7 and 8 show the measured and theoretical radiation pattern curves at the horizontal (H-plane) and vertical (E-plane) cuts, respectively, indicating that the beamwidth of the radiation pattern is as designed. The first nulls are filled and the levels of the first sidelobes are raised from the design value of −33 dB. These effects may be due to an unsatisfactory field distribution in the quiet-zone, due to an incorrect aperture field of the antenna, or due to both of these. For example, a quadratic phase error in either of these may be the cause.

In order to better explain the measured results, additional tests and simulations are carried out. The aperture field of the Odin telescope is measured with the differential phase method [8] in the horizontal or *x*-direction across the centerline of the aperture. The transmitted signal is split with a power divider to two adjacent transmitting pyramidal horns. The horns are scanned three times across the aperture and the powers received by the Odin radiometer are recorded. The three recorded powers are: P_1, only the first horn is transmitting and the second horn is covered with an absorber; P_2, only the second horn is transmitting and the first horn is covered with an absorber; P_{12}, both the horns are transmitting. The phase difference α_d between the two horns can be retrieved as described in [8]

$$\alpha_d = 180° - \arccos\left(\frac{P_1 + P_2 - P_{12}}{2\sqrt{P_1 P_2}}\right). \tag{1}$$

Furthermore, the phase distribution in the aperture can be retrieved from the phase difference between the horns. The distance between the two horns is 65 mm, and the scanning step is 20 mm. The measurement distance from the center-point of the main mirror is about 1 m. Figure 9 shows the powers recorded with three scans. Figure 10 shows the retrieved phase distribution in the aperture of the Odin telescope. The peak-to-peak phase ripple is about 50 degrees in the aperture extent. The measured amplitude and phase ripples are likely to be caused by multiple reflections between the probe horn and the Odin telescope. However, the average of the measured phase is almost flat across the aperture, but the amplitude is asymmetric.

The effects of the imperfect field distributions in the quiet-zone of the CATR and in the aperture of the Odin telescope on the measured radiation pattern are simulated. Figures 11 a and b show the amplitude and phase of the aperture fields (designed and measured) and the quiet-zone field (theoretical with two joints) used in the radiation pattern simulations. Also, an ideal quiet-zone field with flat amplitude and phase distributions is used in the simulations. The designed aperture field has a flat phase distribution and an edge illumination of −17 dB in the amplitude, resulting in the first sidelobe level of −33 dB. The average of the measured amplitude in the left side is almost like the designed amplitude, but in the right side the amplitude taper is noticeably steeper than the designed amplitude taper. This is probably caused by a combination of misalignment of the receiver feed horn and unterminated reflections within the 119 GHz receiver. These problems were later discovered and corrected. The theoretical quiet-zone field with two joints in the hologram structure is considered in the simulations. Theoretical quiet-zone field is used, because the phase of the quiet-zone field cannot be measured. However, the agreement between the measured and theoretical amplitudes is very good (Figure 4 a), and thus, the phase can be assumed to be similar to the theoretical one.

The values of the aperture and the quiet-zone fields within the circular aperture are taken from the field values in one straight line (*x*-axis). The amplitude and phase are interpolated separately by the following equation:

$$A(\rho,\varphi) = A_-(\rho) \cdot (1 - \sin(\varphi)) + A_+(\rho) \cdot (1 + \sin(\varphi)), \tag{2}$$

where $A(\rho,\varphi)$ and $A_\pm(\rho)$ are amplitudes or phases in the circular aperture and in one line, respectively. The sub-index $\pm$ corresponds to field values at the positive or negative *x*-axis. The angle φ is the four-quadrant arctangent $\varphi = \arctan(x, y)$ running from 0 to 2π, and ρ is the distance from the origin.

The radiation patterns can be calculated as given in [9]

$$f(\mathbf{u}_r) = \int\limits_0^b \int\limits_0^{2\pi} e^{jk\mathbf{u}_r \cdot \rho} E_a(\rho,\varphi) g(\rho,\varphi) * \rho \, d\varphi \, d\rho, \tag{3}$$

where $\mathbf{u}_r$ is the unit vector in the direction of the observation point, b is the radius of the aperture, $E_a(\rho,\varphi)$ is the tangential aperture field (ideal or measured), β is the wave number, and $g(\rho,\varphi)$ is the quiet-zone field (ideal or theoretical with two joints).

Figure 12 shows the measured radiation pattern and the three simulated radiation patterns in the H-plane. **A**: The measured radiation pattern, **B**: the aperture field is as designed and the quiet-zone field is ideal, **C**: the aperture field is as designed and the quiet-zone is the theoretical one with two joints in the hologram structure, **D**: the aperture field is interpolated from the measurement at one horizontal line and the quiet-zone field is the theoretical one with two joints.

The increase of the first sidelobe level in the left side caused by the incorrect quiet-zone field is about 4 dB, but in the right side the first sidelobe is at the same level as designed. The more corrupted quiet-zone field, especially the phase, in the right side contributes more to the left side of the radiation pattern. When the measured aperture field is taken into account, the simulated radiation pattern agrees well with the measured one. There is a difference of about 3 dB in the first sidelobe level. The steep amplitude taper in the right hand part of the aperture field is seen as the reason for the high sidelobes in the measurements. The steep amplitude taper affects the radiation pattern on both sides of the radiation pattern. The effects of the imperfect aperture and quiet-zone fields are the increased sidelobe levels and the filled nulls, but the effect on the main lobe is still small.

There are aspects that have to be taken into account when evaluating the practicability and results of the radiation pattern simulations described above. The aperture field scan is not very accurate due to possible reflections, and it is carried out only at one horizontal line across the

aperture. However, these simulations should give reasonable ideas of the causes of the increased sidelobe levels. The real phase distribution of the quiet-zone field may have been more degraded than the simulations of the quiet-zone imply, which may result in an additional increase of the sidelobe levels. A more accurate diagnosis of the differences between the simulated and measured radiation patterns would require a more comprehensive information about the quiet-zone field and the aperture field of the Odin telescope.

4. Conclusions

A 119 GHz CATR based on a 2.4 m × 2.0 m hologram has been described. The design, fabrication, and the results of the theoretical and experimental analysis of the hologram CATR have been presented. The optimized, theoretical peak-to-peak amplitude and phase ripples are less than 1 dB and 10°, respectively. The measured amplitude ripple is 3 dB in the worst part of the quiet-zone and less than 1.5 dB over the most parts of the quiet-zone. The difference between the optimized and measured quiet-zone field is due to the unsatisfactory fabrication procedure: the hologram was fabricated from seven pieces, which could not be perfectly aligned. However, the quiet-zone field quality was appropriate for the tests of the main beam region of the Odin telescope. The measured main lobe of the telescope is symmetric and the beamwidth is as designed. The hologram CATR has shown its applicability at millimeter wavelengths. However, fabrication technologies for the large holograms have to be further developed. The results of the radiation pattern measurement were evaluated by comparing them to the results of the radiation pattern simulations. Misalignment of the Odin telescope feed at the time of the measurement resulted in an asymmetric aperture field, which together with an imperfect quiet-zone field increase the level of the first sidelobe.

References

[1]   J. Tuovinen, A. Vasara, and A. Räisänen, "A new type of compact antenna test range at mm-waves," *Proceedings of the 22nd European Microwave Conference*, Espoo, Finland, August 1992, pp. 503−508.

[2] T. Hirvonen, J. Ala-Laurinaho, J. Tuovinen, and A. Räisänen, "A compact antenna test range based on a hologram," *IEEE Transactions on Antennas and Propagation*, Vol. 45, No. 8, August 1997, pp. 1270–1276.

[3] J. Ala-Laurinaho, T. Hirvonen, and A.V. Räisänen, "On the planarity errors of the hologram of the CATR," *Proceedings of the 1999 AP-S International Symposium*, Orlando, FL, USA, July 1999, pp. 2166–2169.

[4] F. von Schéele, "The Swedish Odin satellite to eye heaven and earth," *47th International Astronautical Congress, IAF*, October 1996.

[5] A. Vasara, J. Turunen, and A. Friberg, "Realization of general nondiffracting beams with computer-generated holograms," *Journal of Optical Society of America A*, Vol. 6, 1989, pp. 1748–1754.

[6] J. Ala-Laurinaho, T. Hirvonen, J. Tuovinen, and A.V. Räisänen, "Numerical modeling of a nonuniform grating with FDTD," *Microwave and Optical Technology Letters*, Vol. 15, No. 3, June 1997, pp. 134–139.

[7] T. Hirvonen, J. Ala-Laurinaho, P. Piironen, J. Tuovinen, and A.V. Räisänen, "A 119 GHz CATR based on a 2.4 m hologram," in *Proceedings of the 19th Meeting and Symposium of AMTA*, Boston, MA, USA, November 1997, pp. 164–169.

[8] A. Lehto, J. Tuovinen, O. Borić, and A.V. Räisänen, "Accurate millimeter wave antenna phase pattern measurements using the differential phase method with three power meters," *IEEE Transactions on Antennas and Propagation*, Vol. 40, No. 7, July 1992, pp. 851–853.

[9] W.L. Stutzman and G.A. Thiele, *Antenna Theory and Design.* New York: John Wiley & Sons, 1981, 598 p.
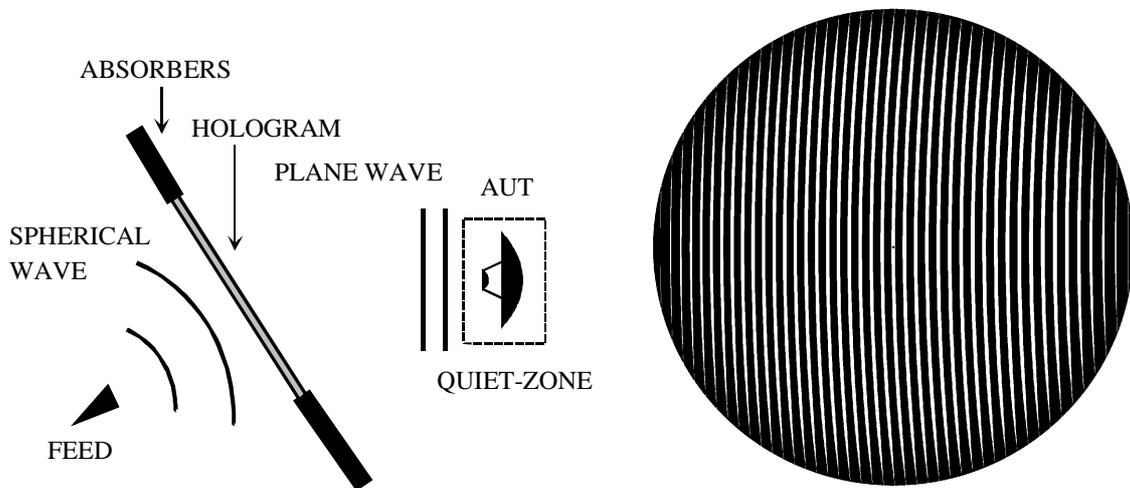
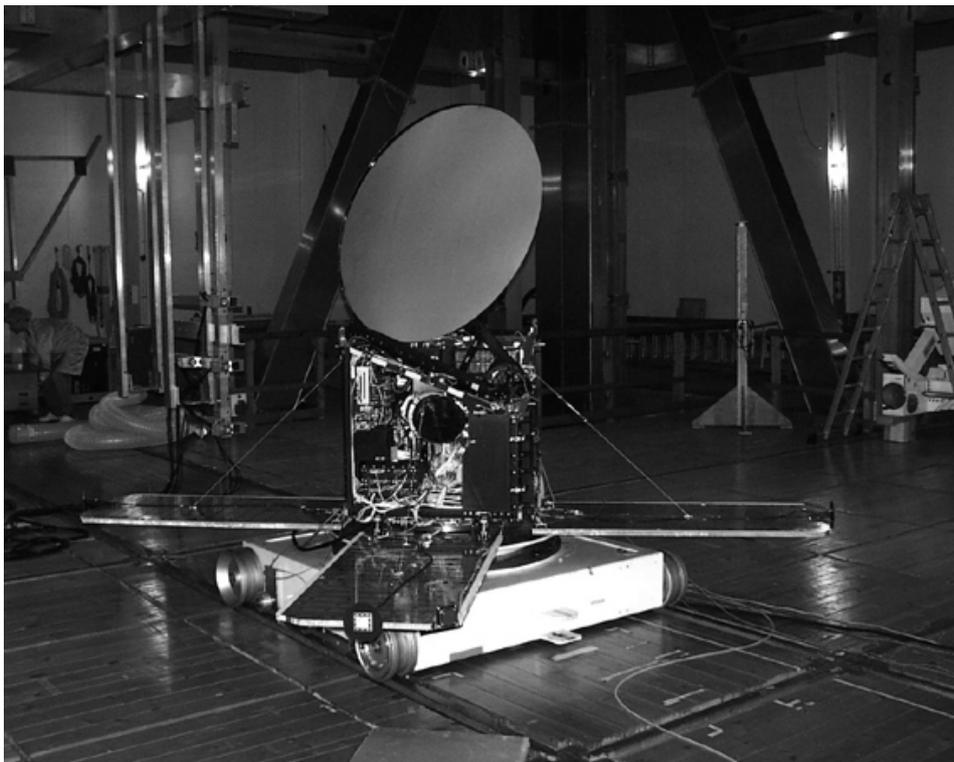*Figure 1. Layout of a hologram CATR and an example of a binary amplitude hologram.*
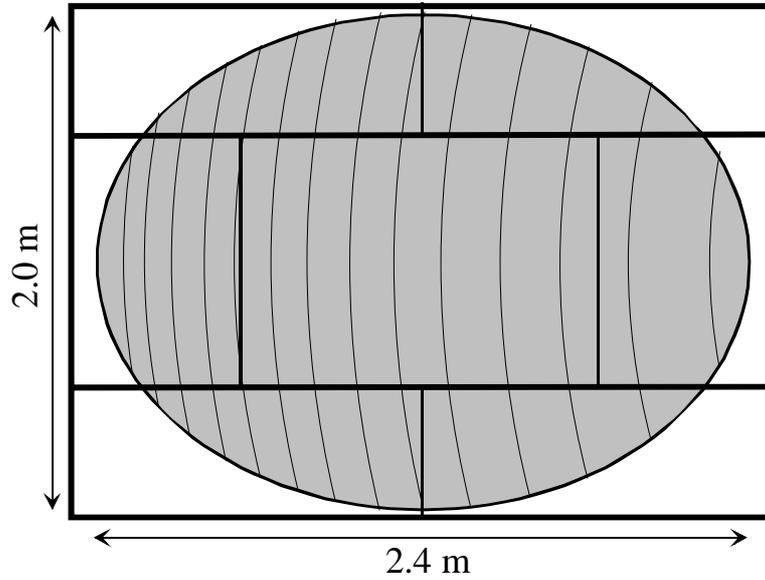

Figure 2. Odin telescope.

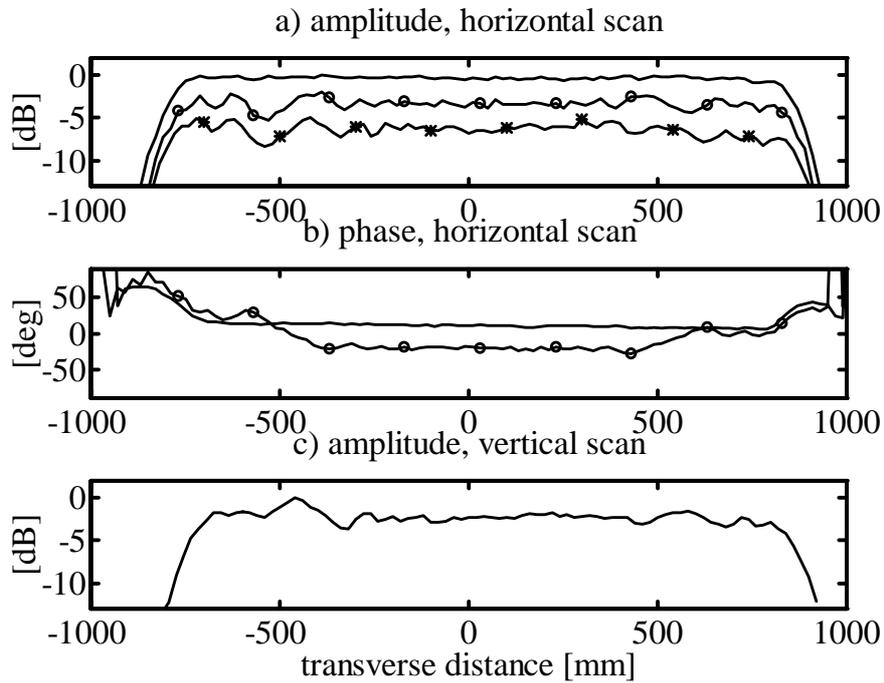*Figure 3. Layout of the hologram for the Odin tests.*

Figure 4. Quiet-zone field. a) Amplitudes in the horizontal direction: optimized theoretical (−), theoretical with the joints (o), and measured (∗), b) phases in the horizontal direction: optimized theoretical (−) and theoretical with the joints (o), c) measured amplitude in the vertical direction ($f = 119$ GHz, vertical polarization).
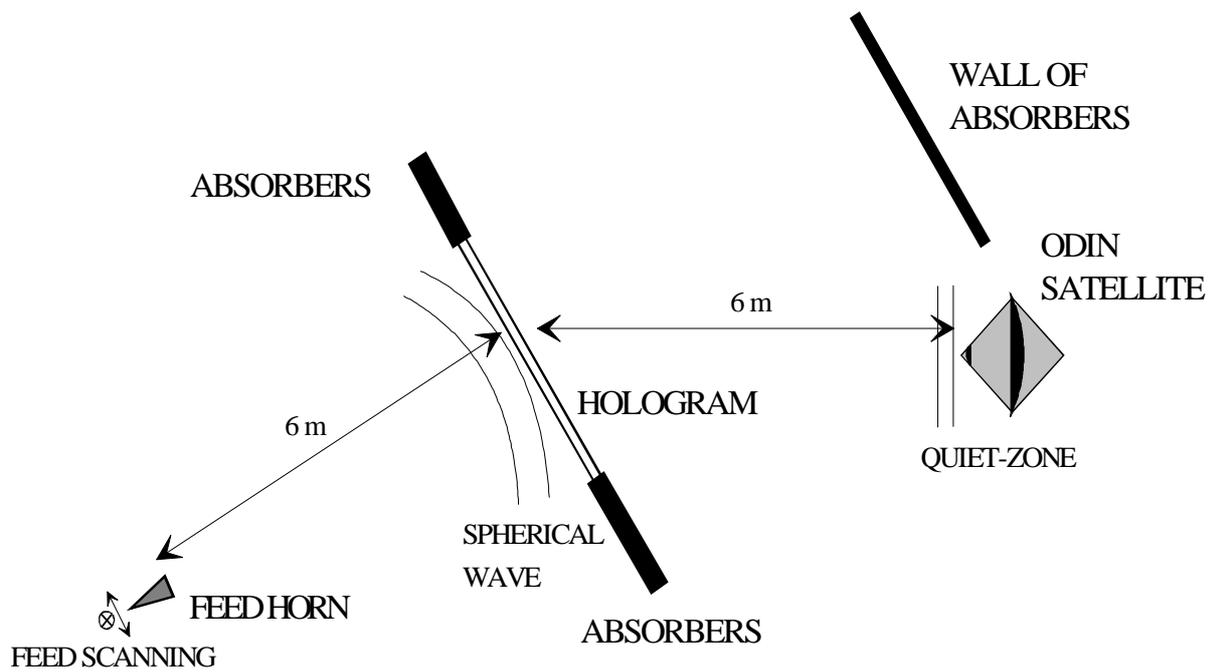
Figure 5. Schematic of the Odin measurement set-up, top view.
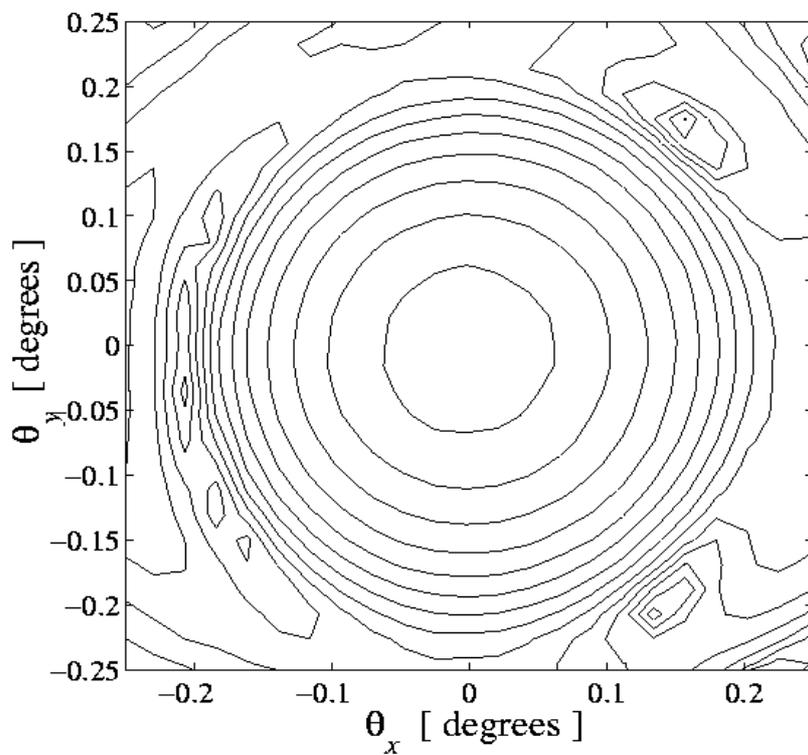
Figure 6. Main beam radiation pattern of the Odin telescope at 119 GHz.
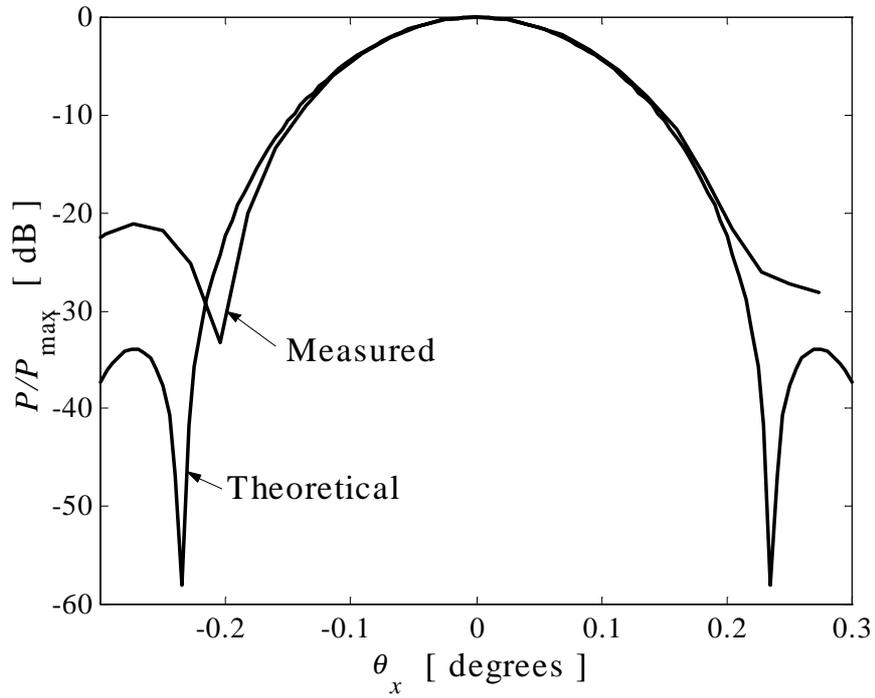
Figure 7. Horizontal (H-plane) cut of the main beam radiation pattern of the Odin telescope.
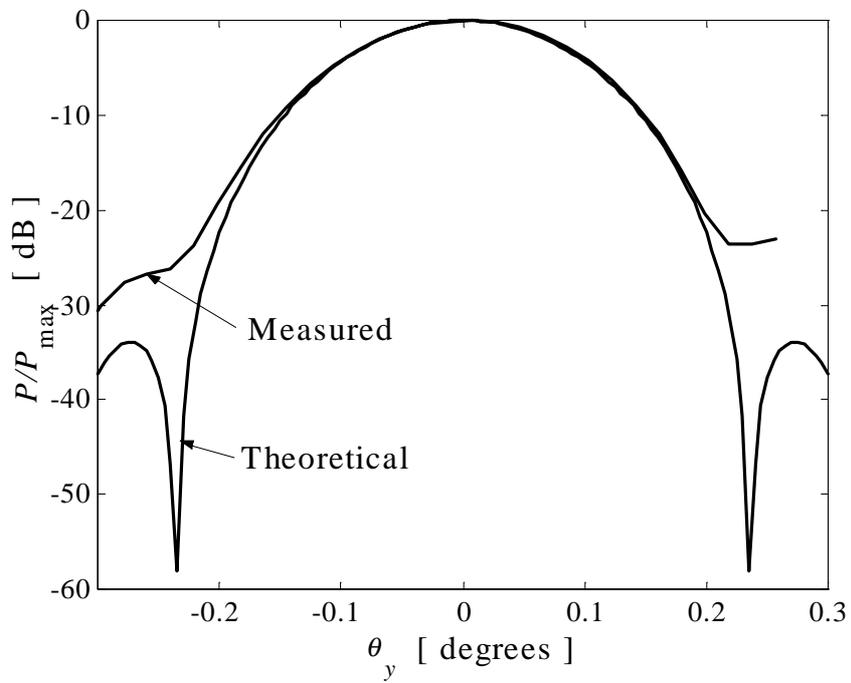

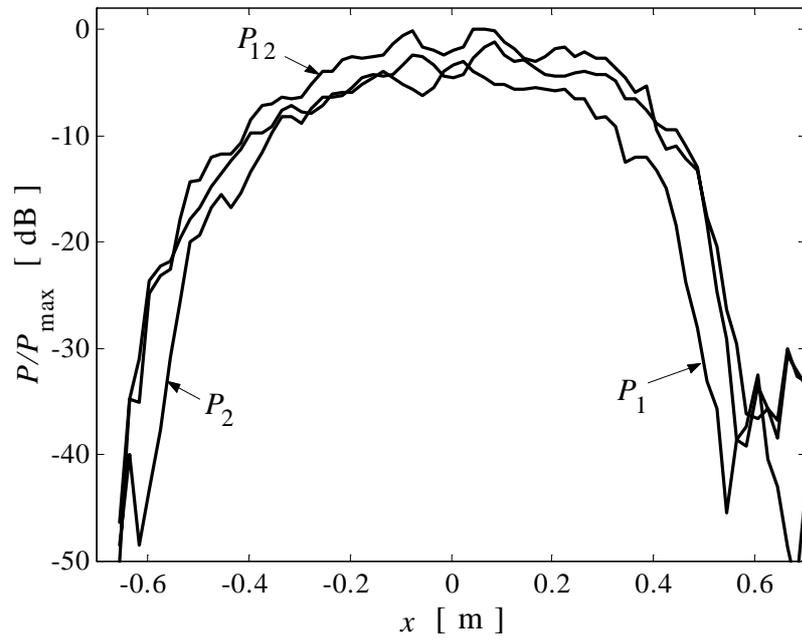*Figure 8. Vertical (E-plane) cut of the main beam radiation pattern of the Odin telescope.*

12

Figure 9. Three horizontal power-scans across the centerline of the aperture.
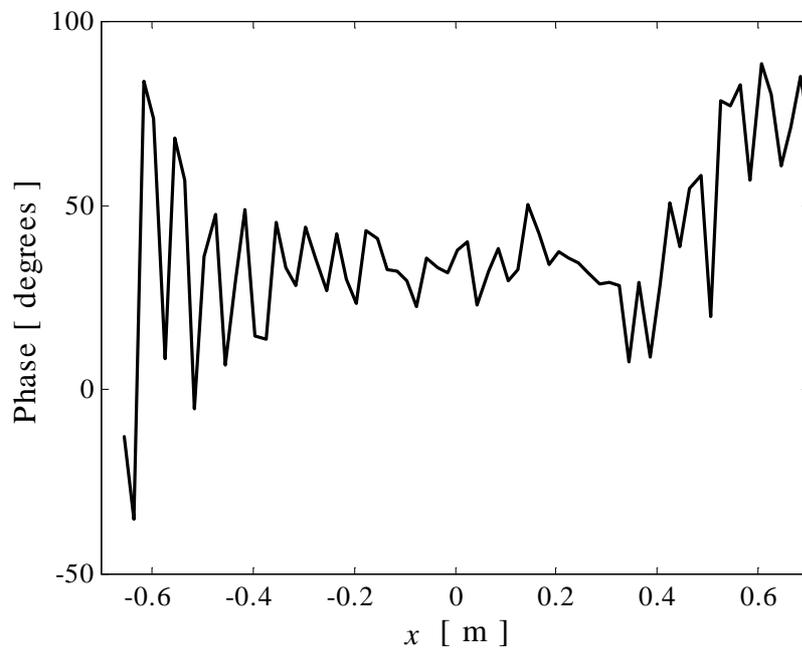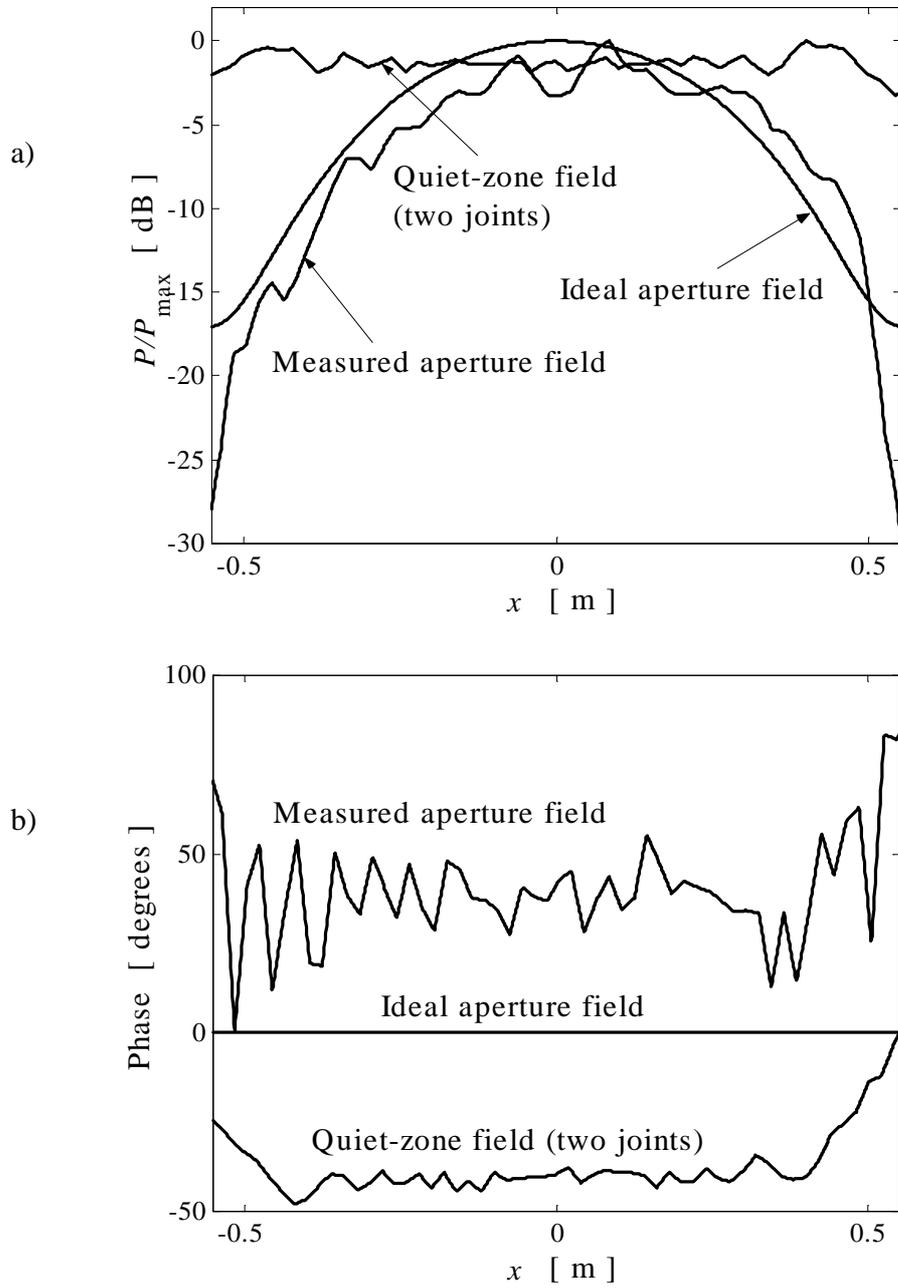

Figure 10. Phase distribution across the centerline of the Odin aperture.

13

Figure 11. a) Amplitudes and b) phases of the aperture and quiet-zone fields used in the radiation pattern simulations.
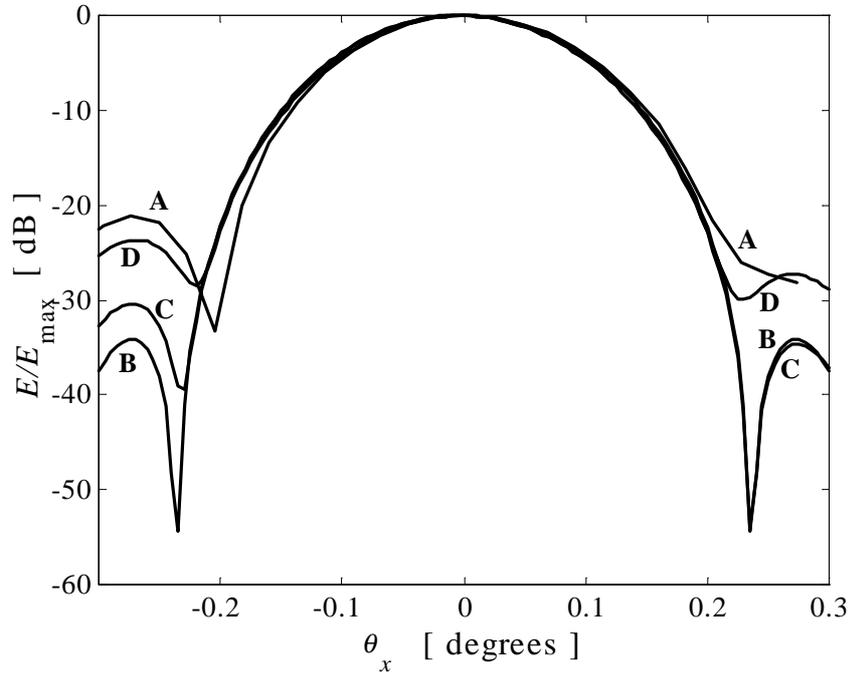
*Figure 12. Measured (**A**) and simulated radiation patterns. **B**: Ideal aperture field and ideal quiet-zone field, **C**: ideal aperture field and theoretical quiet-zone field, **D**: interpolated aperture field based on a centerline measurement and theoretical quiet-zone field.*